J E M T
Journal of Earth and Marine Technology
homepage URL: ejurnal.itats.ac.id/jemt

Computational Fluid Dynamic for Performance Hydrofoil due to Angle of Attack

Maria Margareta Zau Beu [1]
[1] Department of Naval Architecture and Shipbuilding, Institut Teknologi Adhi Tama Surabaya
e-mail: maria_margaret@itats.ac.id
DOI: 10.31284/j.jemt.2020.v1i1.1146

Article info
Received:
13 May 2020
Revised:
11 August 2020
Accepted:
15 August 2020
Published:
3 September 2020

Keywords:
Computational fluid dynamic (CFD), hydrofoil, angle of attack (AoA)

Abstract

This study uses a 2-D computational fluid dynamic (CFD) with a hydrofoil object. The general parameters used are pressure-based with Reynold numbers (Re) 106. The Pressure velocity coupling method used is SIMPLE with Reynold k-ε as the viscous model on ANSYS Fluent 2019R1. The angle of attack variations are used starting from 00, 20, 40, 60, 10, 120, 150, 200, 250, and 300. From the simulation shows the hydrofoil characters depicted in the Coefficient drag (CD), Coefficient Lift (CL) and Pressure graphs Coefficient (CP) approaches the experimental results.

1. Introduction

Hydrofoil was first introduced by Forlanini, who in 1906 demonstrated a ship that moved 1.65 tons reaching a speed of 38 knots with 75-hp, which compares favorably with the modern craft. To achieve better performance, hydrofoil with higher lift coefficients and higher lift-to-drag ratios are most desired [1]. The hydrofoil usually consists of a wing-like structure mounted on struts below the hull, or across the keels of a catamaran in a variety of boats. At present several hundred hydrofoil craft are in service throughout the world. Experiments have been carried out in wind tunnels show that as speed increases on water boats equipped with hydrofoil, the hydrofoil element under the hull develops enough lift to lift the hull out of the water, which greatly reduces the hull resistance. This provides an increase in speed and fuel efficiency accordingly. Experiments at the wind tunnel, computer mathematic, and simulation using computers have all played important roles in hydrofoil development.

2. Literature Review

Computer Fluid Dynamics (CFD) is like a virtual wind tunnel and while it offers much more than just a testing facility on the computer, it is mainly used is certainly in the analysis of flow around a given design and there are clear analogies [2]. CFD has indeed become a powerful tool to be employed either for applied research and industrial applications. Computational simulations and analyses are increasingly performed in many fluid engineering applications. However, several factors influence CFD simulation results, namely the experience and knowledge of the operator or user about CFD, adequate computer specifications, domain shape determination, meshing grid type and size, turbulent models, and others [2-6]. Hydrofoil studies with variations in the entry angle and form factor were also conducted [7] where the results showed there is a maximum point of C_L to the variation of the angle of attack which is a stall phenomenon that occurred in the angle of 20^0 in each of NACA foil type. Besides, The maximum lift is increased by increasing the depth ratio from $h/c = 1$ to $h/c = 4$ [8]. The system drag coefficients and lift coefficient were found by using FLUENT [9-10]. The computations were based on the Reynolds-averaged Navier-Stokes equations, which were solved with the standard k-ε turbulence model. The standard wall function was adopted for the flow near the solid wall. The SIMPLE (semi-implicit method for the pressure linked equations) algorithm was employed for nonlinear iterations

between the velocity and pressure fields [11]. The iterative formulations of the SIMPLE methods generally exhibit better behavior [12]. SIMPLE typically converges very fast and efficiently, but for industrial flows in complex geometries and with marginal flow stability, convergence may stall.

3. Research Method

3.1 Computational Approach

Computational fluid dynamics (CFD) is based on three basic physical principles: conservation of mass, momentum, and energy. The governing equations in CFD are based on these conservation principles. The continuity equation 2-D is based on the conservation of mass for an incompressible fluid.

$$\frac{\partial \phi}{\partial t}+\frac{\partial (u\phi)}{\partial x}+\frac{\partial (v\phi)}{\partial y}=0 \quad (1)$$

The turbulence model widely used in CFD is k-ε model. The transported turbulent quantities of the k-ε model have physical meaning. The first variable is the turbulent kinetic energy *k*

$$k=\frac{1}{2}(\overline{u'u'}+\overline{v'v'}+\overline{w'w'}) \quad (2)$$

The second variable is the viscous dissipation rate ε which governs the dissipation of turbulent kinetic energy due to the shearing of the smallest eddies

$$\varepsilon = 2\nu\overline{e'_{ij}\, e'_{ij}} \quad (3)$$

ε is given per unit mass. A velocity scale can conveniently be taken from $u_{ref}\sqrt{k}$, similarly, a length scale is obtained from $l=k^{3/2}/\varepsilon$ and the eddy viscosity then becomes

$$\mu_T=\rho C\mu l u_{ref}=\rho C\mu \frac{k^2}{\varepsilon} \quad (4)$$

When $C\mu, \sigma_k, \sigma_{\varepsilon,} C_{\varepsilon 1}$ and $C_{\varepsilon 2}$. These constants have been arrived at by comprehensive data fitting for a wide range of turbulent flows,

$C\mu = 0{,}09, \sigma_k = 1.0, \sigma_e = 1.3, C_{\varepsilon 1} = 1.44, C_{\varepsilon 2} = 1.92$

For the k-ε model incoming turbulence was specified through turbulent intensity at 5% and turbulent viscosity ratio at a value of 10.

3.2 Lift and Drag Coefficient

Lift is generated on a foil in a flow, the force working in the normal direction on the flow. The magnitude of the angle of the lift will depend on the angle of attack, the thickness, hydrofoil, and the camber. In addition to the lift force, there will be a drag force that works in the flow direction, this is mostly due to viscous effects.

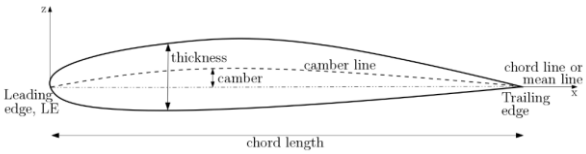

Figure 1. 2D-foil geometry definition[13]

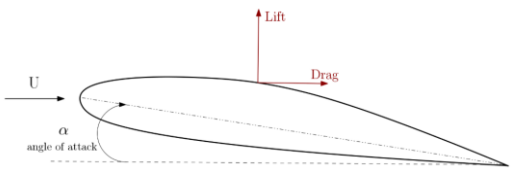

Figure 2. 2D-foil with the angle of attack [13]

$$C_L=\frac{2L}{\rho_{water}U^2A} \quad (5)$$

$$C_D=\frac{2D}{\rho_{water}U^2A} \quad (6)$$

where the characteristic area A corresponds to the hydrofoil planform area for a horizontally oriented, completely submerged hydrofoil. Value for pressure coefficient (C_P) is,

$$C_P = \frac{P - P_\infty}{0.5\rho_\infty V_\infty^2} = \frac{P - P_\infty}{P_0 - P_\infty} \quad (7)$$

Where, P is the static pressure at the point at which the pressure coefficient is being evaluated, P_∞ is the static pressure in the freestream, P_0 is the stagnation pressure in the freestream, ρ_∞ is the freestream fluid density, V_∞^2 is the freestream velocity of the fluid, or the velocity of the body through the fluid [14-15].

3.3 Geometry and Mesh Generation

The geometry of the hydrofoil is shown in figure 3. Topologies of the domain are used C-meshes and structured grids. The mesh quality at the trailing edge in the C-mesh is quite good with nearly orthogonal cells.

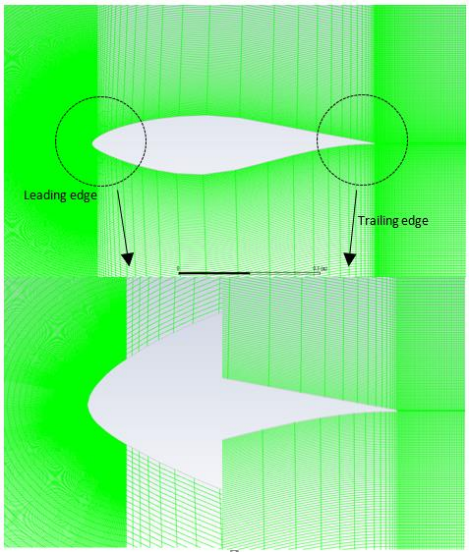

Figure 3. The geometry of hydrofoil and mesh of the computational domain

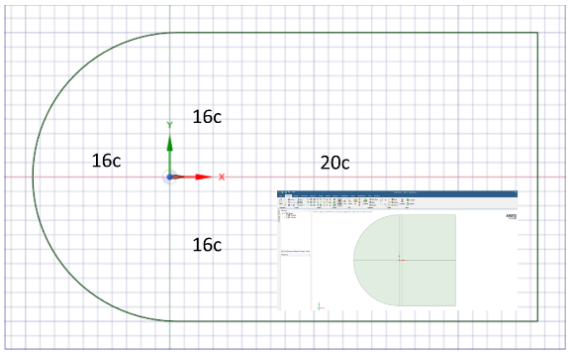

Figure 4. Dimension of domain

A schematic view of the domain is shown in figure 4. The size of the domain is radius R=16c, length L=20c, and height H=16c+16c. Where c is chord length. Figure 3 shown the mesh around the leading edge and trailing edge. The grids are about 200 thousand cells, with the smallest cell size 2.4e-002 m.

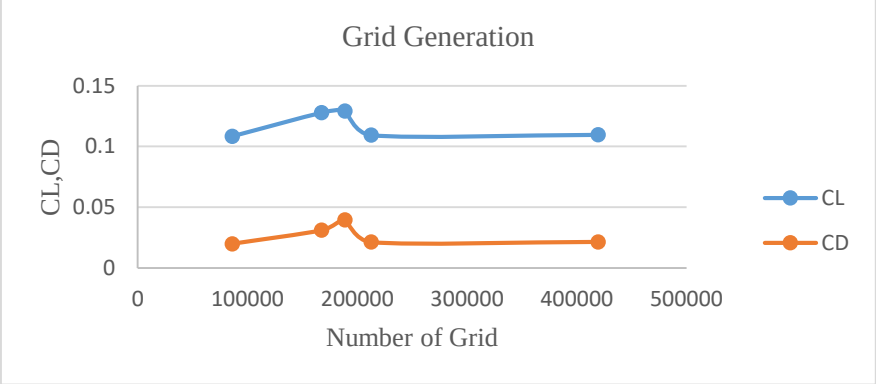

Figure 5. Grid generation

The problem consists of flow around the hydrofoil at various angles of attack-α (0^0, 2^0, 4^0, 6^0, 1^0, 12^0, 15^0, 20^0, $25^{0,}$ and 30^0) [16-18]. The inputs and boundary conditions are presented in table 1.

Table 1. Inputs and Boundary Condition

General Parameter	
Solver	Pressure based
State	Steady
Viscous Model	Reynold k-epsilon (ε)
Material	Water
Density	1000 kg/m^3
Reynold Number (Re)	10^6
Inlet Velocity	10 knot
Chord Length	1 m
Pressure-Velocity Coupling	SIMPLE

4. Result and Analysis

The numerical method used here had been validated in the experimental study. The result is presented in Figures 26 and 27.

4.1 Contour Velocity and Pressure Coefficient

Hydrofoil performance obtained through the CFD approach with a fluid (water) velocity of 5.14 m/s or equivalent to 10 knots with variations angle of attack (AoA)-α, shows the boundary layer and wake increase in thickness with increasing angle of attack. The pressure coefficient of the hydrofoil's upper surface was positive and the lower surface was negative. The coefficient of pressure difference is much larger on the leading edge, while on the rear/trailing edge it was much lower.

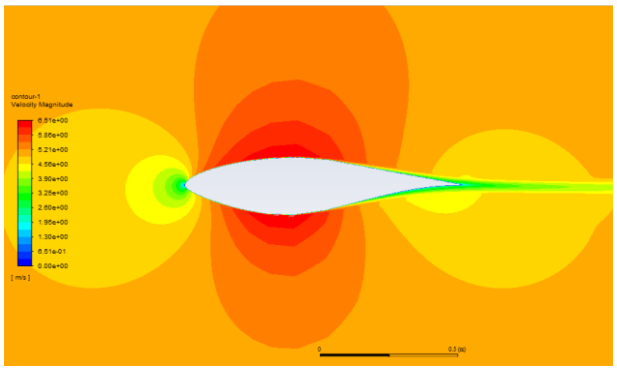

Figure 6. Contour Velocity at AoA 0^0

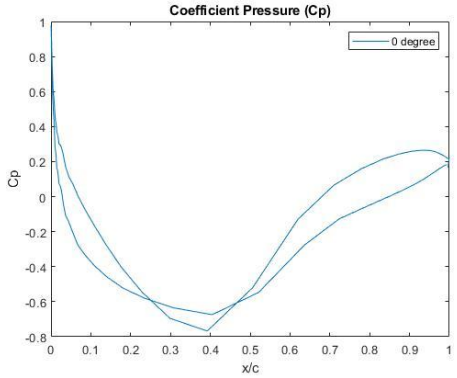

Figure 7. Coefficient Pressure (C_P) at AoA 0^0

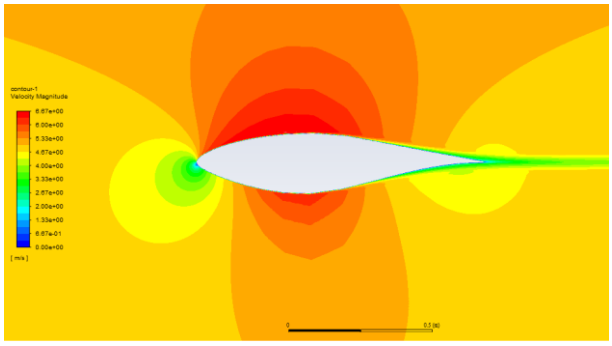

Figure 8. Contour Velocity at AoA 2^0

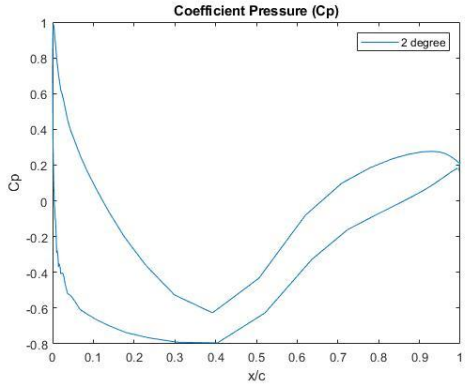

Figure 9. Coefficient Pressure (C_P) at AoA 2^0

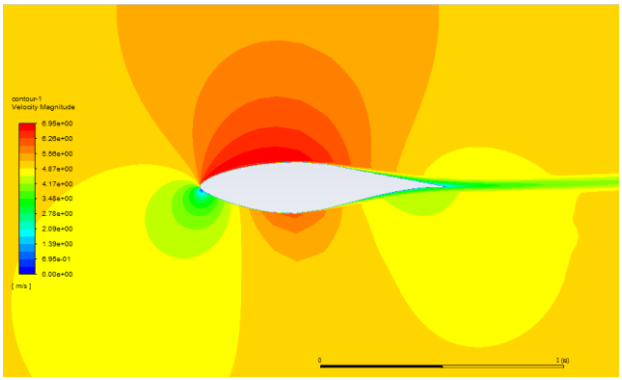

Figure 10. Contour Velocity at AoA 4^0

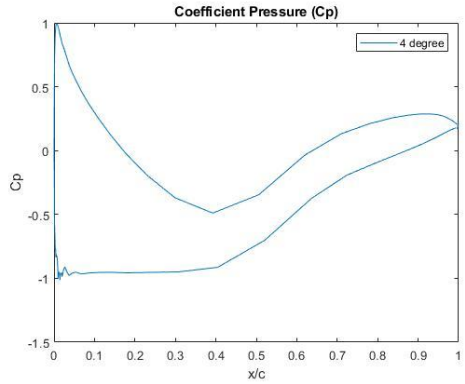

Figure 11. Coefficient Pressure (C_P) at AoA 4^0

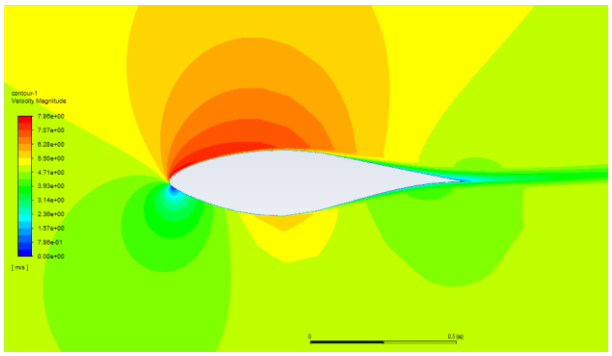

Figure 12. Contour Velocity at AoA 6^0

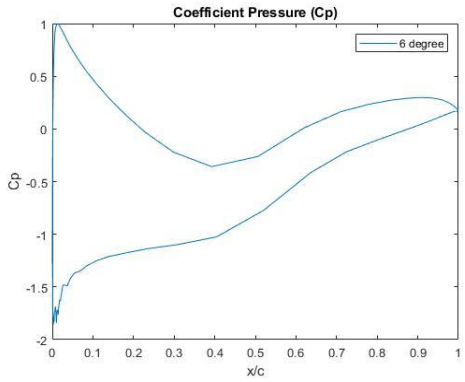

Figure 13. Coefficient Pressure (C_P) at AoA 6^0

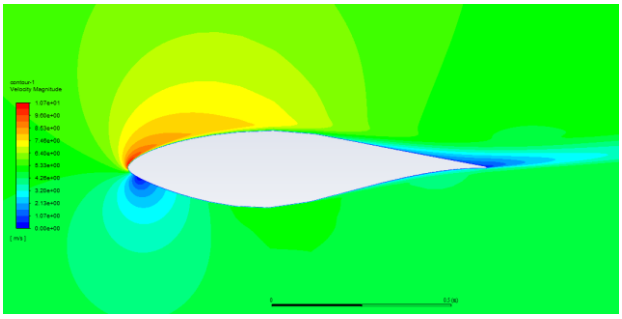

Figure 14. Contour Velocity at AoA 10^0

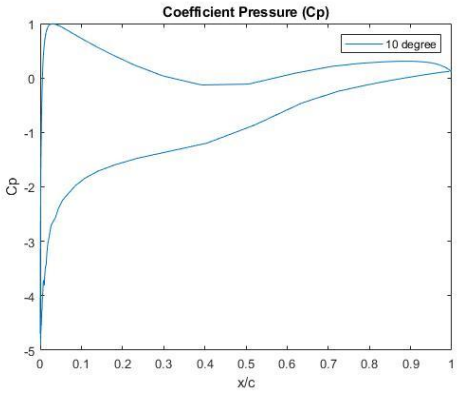

Figure 15. Coefficient Pressure (C_P) at AoA 10^0

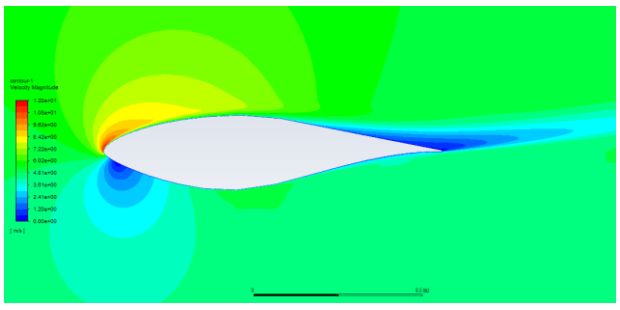

Figure 16. Contour Velocity at AoA 12^0

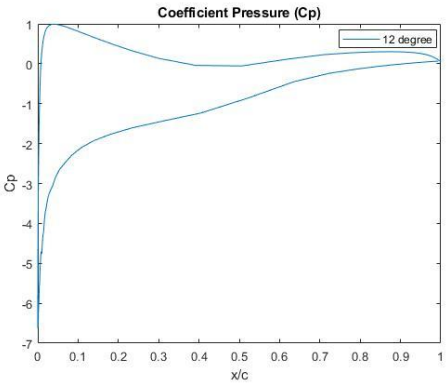

Figure 17. Coefficient Pressure (C_P) at AoA 12^0

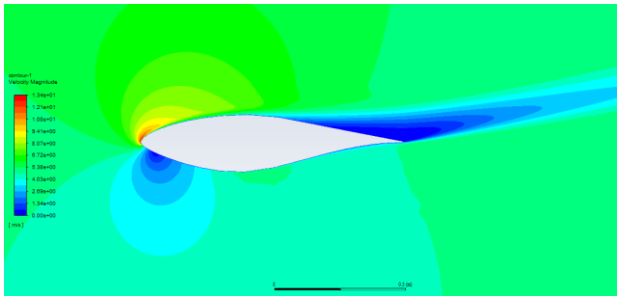

Figure 18. Contour Velocity at AoA 15^0

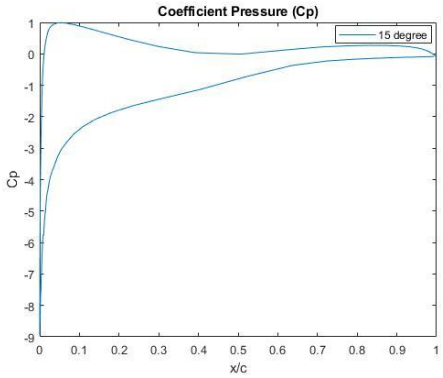

Figure 19. Coefficient Pressure (C_P) at AoA 15^0

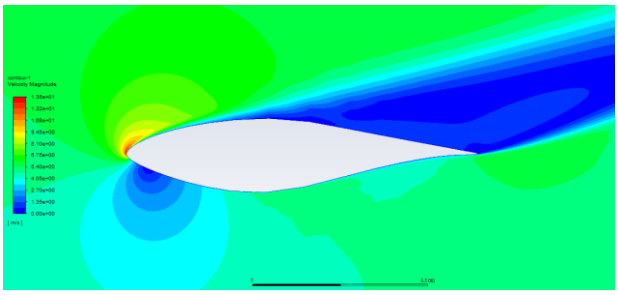

Figure 20. Contour Velocity at AoA 20

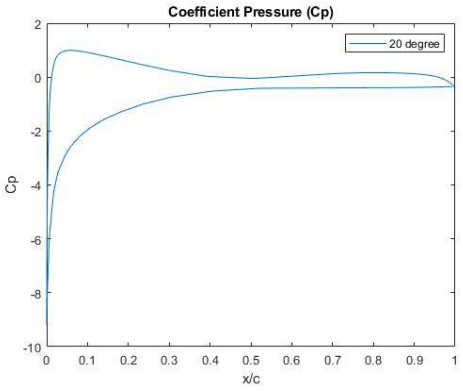

Figure 21. Coefficient Pressure (C_P) at AoA 20^0

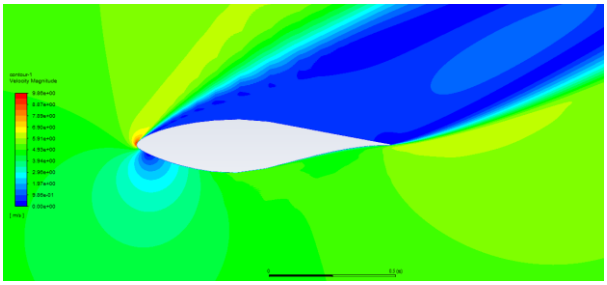

Figure 22. Contour Velocity at AoA 25^0

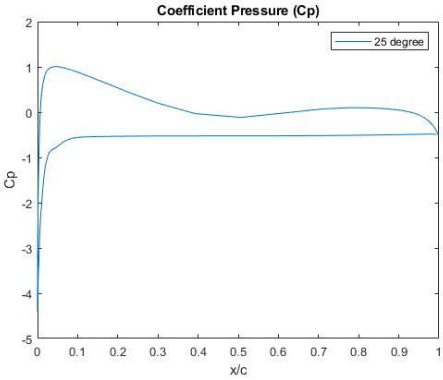

Figure 23. Coefficient Pressure (C_P) at AoA 25^0

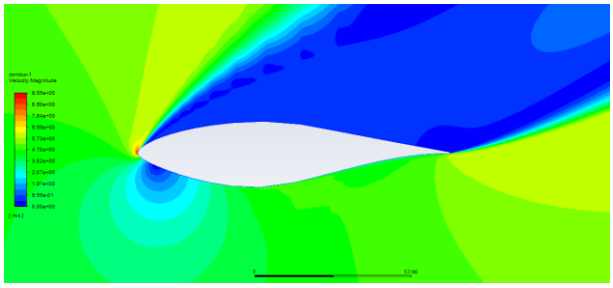

Figure 24 Contour Velocity at AoA 30^0

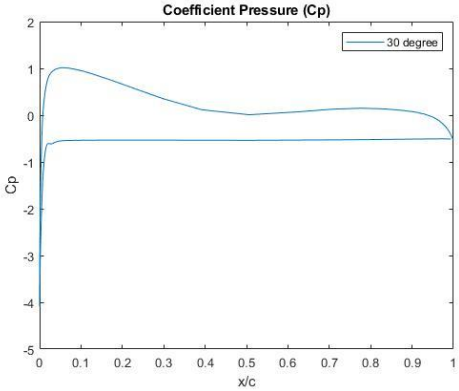

Figure 25. Coefficient Pressure (C_P) at AoA 30^0

The invalidation test case, the lift, and the drag coefficients are compared with experimental data. Viscous model k-ε turbulence show very good agreement for the angle of attack of up to about 0^0-15^0 and 20^0-25^0 stalls occur and increase again at an angle of attack 30^0.

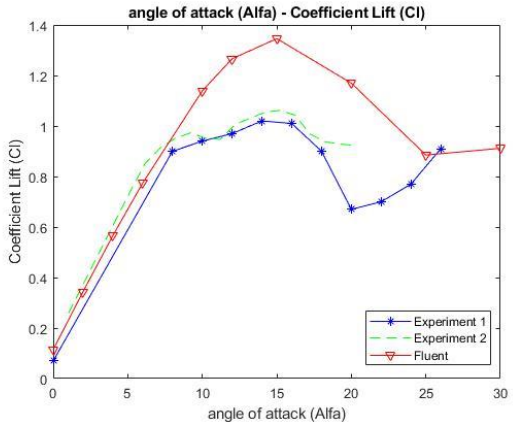

Figure 26. Lift Coefficient (C_L) for Hydrofoil in Various of Angle of Attack

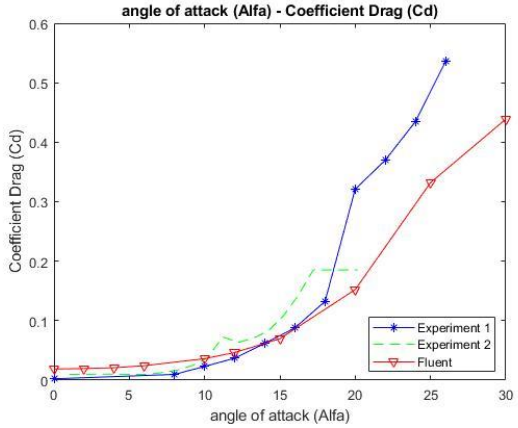

Figure 27. Drag Coefficient (C_D) for Hydrofoil in Various of Angle of Attack

Difference values from experiments and CFD simulations, for the lift coefficient (C_L), the average error is obtained 0.1337 and for the drag coefficient (C_D) average error is obtained 0.0374.

6. Conclusion

From the result and analysis, 2D-hydrofoil simulation with the angle of attack variations are used starting from 0^0, 2^0, 4^0, 6^0, 1^0, 12^0, 15^0, 20^0, 25^0, and 30^0 with the constant Reynolds number 10^6 using realized k-ε turbulence model. The Pressure velocity coupling method used is SIMPLE. It is seen that with the help of CFD Ansys-Fluent software, successful analysis of the Hydrofoil performance has been carried at various angles of attack (AoA) - α (0^0, 2^0, 4^0, 6^0, 10^0, 12^0, 15^0, 20^0, 25^0, 30^0) with constant Reynolds number 10^6 using the k-ε turbulence model. The boundary layer and wake increase in thickness with increasing angle of attack. In future works, more realistic environmental hydrodynamic conditions will be considered for practical investigation, including the shear flow with an exponential profile and the free-surface waves.

Acknowledgment

The numerical study was conducted at Departement System Engineering and Naval Architecture, National Taiwan Ocean University, Taiwan. The university provides facilities and support during the research.

References

[1] Müller, J. D. (2015). Essentials of computational fluid dynamics. In *Essentials of Computational Fluid Dynamics*. https://doi.org/10.5860/choice.196614

[2] Zau Beu, M. M., & Kusuma, I. P. A. I. (2017). Investigasi Numerik VIV (Vortex Induced Vibration) Pada Diameter Kabel Hydrophone 0.04 M Sistem Akustik Bawah Air. *ROTOR*, *10*(2), 47. https://doi.org/10.19184/rotor.v10i2.6387

[3] Pranatal, E., & Beu, M. M. Z. (2018). Analisa CFD Penggunaan Duct pada Turbin Kombinasi Darrieus-Savonius. *Jurnal IPTEK*. https://doi.org/10.31284/j.iptek.2018.v22i1.239

[4] Marchand, J. B., Astolfi, J. A., & Bot, P. (2017). Discontinuity of lift on a hydrofoil in reversed flow for tidal turbine application. *European Journal of Mechanics, B/Fluids*, *63*, 90–99. https://doi.org/10.1016/j.euromechflu.2017.01.016

[5] Liu, Z., Qu, H., & Shi, H. (2019). Performance evaluation and enhancement of a semi-activated flapping hydrofoil in shear flows. *Energy*, *189*, 116255. https://doi.org/10.1016/j.energy.2019.116255

[6] Stern, F., Wang, Z., Yang, J., Sadat-Hosseini, H., Mousaviraad, M., Bhushan, S., Grenestedt, J. L. (2015). Recent progress in CFD for naval architecture and ocean engineering. Journal of Hydrodynamics, 27(1), 1–23. https://doi.org/10.1016/S1001-6058(15)60452-8
[7] Putranto, T., & Sulisetyono, A. (2017). Lift-drag coefficient and form factor analyses of hydrofoil due to the shape and angle of attack. *International Journal of Applied Engineering Research*, *12*(21), 11152–11156
[8] Amini, Y., Kianmehr, B., & Emdad, H. (2019). Dynamic stall simulation of a pitching hydrofoil near free surface by using the volume of fluid method. *Ocean Engineering*. https://doi.org/10.1016/j.oceaneng.2019.106553
[9] ANSYS-Fluent 2019R1 *software*
[10] Elmekawy, A. N., Introduction to ANSYS Meshing Module-01
[11] Wu, J. T., Chen, J. H., Hsin, C. Y., & Chiu, F. C. (2019). Dynamics of the FKT System with Different Mooring Lines. *Polish Maritime Research*, *26*(1), 20–29. https://doi.org/10.2478/pomr-2019-0003
[12] Vandoormaal, J.P., Raithby, G.D., 1984. Enhancements of the SIMPLE method for predicting incompressible fluid flows. Numer. Heat Transf. 7, 147–163.
[13] Dagestad, I. (2018). *Actuation moments for hydrofoil flaps*, Norwegian University of Science and Technology, Department of Marine Technology
[14] Newman, J. N., (1977). Marine Hydrodynamics, MIT.
[15] White, F.M., 2011. Fluid Mechanics, seventh ed. McGraw-Hill, New York, USA.
[16] Giesing, J.P., Smith, A.M.O., 1967. Potential flow about two-dimensional hydrofoils. J. Fluid Mech. 28, 113–129
[17] Ni, Z., Dhanak, M., & Su, T. chow. (2019). Performance of a slotted hydrofoil operating close to a free surface over a range of angles of attack. *Ocean Engineering*, *188*(June), 106296. https://doi.org/10.1016/j.oceaneng.2019.106296
[18] Bai, K.J., 1978. A localized finite-element method for two-dimensional steady potential flows with a free surface. J. Ship Res. 22, 216–230.